Eur. Phys. J. C (2014) 74:3142
DOI 10.1140/epjc/s10052-014-3142-6

THE EUROPEAN PHYSICAL JOURNAL C

Regular Article - Theoretical Physics

Inert doublet dark matter with an additional scalar singlet and 125 GeV Higgs boson

Amit Dutta Banik[a], **Debasish Majumdar**[b]

Astroparticle Physics and Cosmology Division, Saha Institute of Nuclear Physics, 1/AF Bidhannagar, Kolkata 700064, India

Received: 3 September 2014 / Accepted: 20 October 2014

Abstract In this work we consider a model for particle dark matter where an extra inert Higgs doublet and an additional scalar singlet is added to the Standard Model (SM) Lagrangian. The dark matter candidate is obtained from only the inert doublet. The stability of this one component dark matter is ensured by imposing a Z_2 symmetry on this additional inert doublet. The additional singlet scalar has a vacuum expectation value (VEV) and mixes with the Standard Model Higgs doublet, resulting in two CP even scalars h_1 and h_2. We treat one of these scalars, h_1, to be consistent with the SM Higgs-like boson of mass around 125 GeV reported by the LHC experiment. These two CP even scalars contribute to the annihilation cross section of this inert doublet dark matter, resulting in a larger dark matter mass region that satisfies the observed relic density. We also investigate the $h_1 \to \gamma\gamma$ and $h_1 \to \gamma Z$ processes and compared these with LHC results. This is also used to constrain the dark matter parameter space in the present model. We find that the dark matter candidate in the mass region 60–80 GeV ($m_1 = 125$ GeV, mass of h_1) satisfies the recent bound from LUX direct detection experiment.

1 Introduction

The existence of a newly found Higgs-like scalar boson of mass about 125 GeV has been reported by recent LHC results. ATLAS [1] and CMS [2] independently confirmed the discovery of a new scalar and measured signal strengths of the Higgs-like scalar to various decay channels separately. ATLAS has reported a Higgs to diphoton signal strength ($R_{\gamma\gamma}$) of about $1.57^{+0.33}_{-0.29}$ at 95 % CL [3]. On the other hand best fit value of Higgs to diphoton signal strength reported by CMS [4] experiment is $\sim 0.78^{+0.28}_{-0.26}$ for 125 GeV Higgs boson. Despite the success of the Standard Model (SM) of particle physics, it fails to produce a plausible explanation of dark matter (DM) in modern cosmology. The existence of dark matter is now established by the observations such as rotation curves of spiral galaxies, gravitational lensing, analysis of cosmic microwave background (CMB) etc. The DM relic density predicted by the PLANCK [5] and WMAP [6] results suggests that about 26.5 % of our Universe is constituted by DM. The particle constituent of dark matter is still unknown and the SM of particle physics appears to be inadequate to address the issues regarding dark matter. The observed dark matter relic density reported by CMB anisotropy probes suggests that a weakly interacting massive particle or WIMP [7,8] can be assumed to be a feasible candidate for dark matter. Thus, in order to explain dark matter in the Universe one should invoke a theory beyond SM and in this regard a simple extension of the SM scalar or fermion sector or both could be of interest for addressing the problem of a viable candidate of dark matter and dark matter physics. There are other theories though beyond the Standard Model (BSM) such as the elegant theory of Supersymmetry (SUSY) in which the dark matter candidate is supposedly the LSP or lightest SUSY particle which is the superposition of neutral gauge bosons and a Higgs boson [9]. Extra dimension models [10] providing Kaluza–Klein dark matter candidates are also explored at length in the literature. The extension of SM with an additional scalar singlet where a discrete Z_2 symmetry stabilizes the scalar is studied elaborately in earlier works such as [11–23]. It is also demonstrated by the previous authors that a singlet fermion extension of SM can be a viable candidate of dark matter [24–26]. SM extensions with two Higgs doublets (or triplet) and a singlet are addressed earlier where the additional singlet is the proposed dark matter candidate [27–29]. Among various extensions of SM, another simple model is to introduce an additional SU(2) scalar doublet which produces no VEV. The resulting model, namely the Inert Doublet Model (IDM), provides a

[a] e-mail: amit.duttabanik@saha.ac.in

[b] e-mail: debasish.majumdar@saha.ac.in

Published online: 11 November 2014

viable explanation for DM. The stability of this inert doublet is ensured by a discrete Z_2 symmetry and the lightest inert particle (LIP) in this model can be assumed to be a plausible DM candidate. The phenomenology of IDM has been elaborately studied in the literature such as [30–40]. In the case of IDM the lightest inert particle of the inert doublet serves as a potential DM candidate and the SM Higgs doublet provides the 125 GeV Higgs boson consistent with the ATLAS and CMS experimental findings. However, the possibility of having a non-SM Higgs-like scalar that couples very weakly to the SM sector is not ruled out and has been studied extensively in the literature involving two Higgs doublet model (THDM) and models with a singlet scalar where the additional Higgs doublet or the singlet provide the new physics scenario associated with it. Since IDM framework contains two Higgs doublets of which one is the SM Higgs doublet and the other is the dark Higgs doublet which is odd under the discrete Z_2 symmetry (to explain the DM phenomenology), it does not provide any essence of non-SM Higgs. The simplest way to address the flavor of new physics from non-SM Higgs in IDM is to assume a singlet like scalar with non-zero VEV which eventually mixes with the SM Higgs. One may also think of another possibility, where a third Higgs doublet with non-zero VEV is added to the IDM. However, the study of such a model including three Higgs doublets will require too many parameters and fields to deal with which is rather inconvenient and difficult. Hence, in order to study the very effect of non-SM Higgs in IDM and Higgs phenomenology, we consider a minimal extension of IDM with an additional singlet scalar. In this work, we consider a two Higgs doublet model (THDM) with an additional scalar singlet, where one of the two Higgs doublets is identical to the inert doublet, i.e., it assumes no VEV and all the SM sector including the newly added singlet are even under an imposed discrete symmetry (Z_2) while the inert doublet is odd under this Z_2 symmetry. Inert scalars do not interact with SM particles and LIP can be treated as a potential DM candidate. We intend to study and explore how the simplest extension of IDM due to the insertion of a scalar singlet could enrich the phenomenology of Higgs sector and DM sector as well. The signal strength of SM Higgs to any particular channel will change due to the mixing between SM Higgs doublet and the newly added singlet scalar. Inert charged scalars of the inert doublet will also contribute to the $h \to \gamma\gamma$ and $h \to \gamma Z$ channels of SM Higgs. We thus test the credibility of our model by calculating the $R_{\gamma\gamma}$ for $h \to \gamma\gamma$ signal and comparing the same with those given by LHC experiment.

Various ongoing direct detection experiments such as XENON100 [41], LUX [42], CDMS [43,44] etc. provide upper limits on dark matter-nucleon scattering cross sections for different possible dark matter mass. The CDMS [43,44] experiment also claimed to have observed three potential signals of dark matter at low mass region (∼8 GeV). Direct detection experiments such as DAMA [45,46], CoGeNT [47] and CRESST [48] provide bounds on dark matter-nucleon scattering cross sections for different dark matter masses. These experiments conjecture the presence of low mass dark matter candidates. But their results contradict XENON100 or LUX results since both the experiments provide bounds for dark matter-nucleon scattering cross section much lower than those given by CDMS, CRESST or DAMA experiments.

As mentioned earlier, in this work, we consider an Inert Doublet Model (IDM) along with an additional singlet scalar field S. We impose a discrete Z_2 symmetry, under which all SM particles and the singlet scalar S are even while the inert doublet is odd. This ensures the stability of the LIP (denoted as H) of the inert doublet to remain stable and serve as a viable dark matter candidate. Additional scalar singlet having a non-zero VEV mixes with the SM Higgs, provides two CP even Higgs states. We consider one of the scalars, h_1, to be the SM-like Higgs. Then h_1 should be compatible with SM Higgs and one can compare the relevant calculations for h_1 with the results from LHC experiment. The model parameter space for the dark matter candidate is first constrained by theoretical conditions such as vacuum stability, perturbativity, unitarity, and then by the relic density bound given by PLANCK/WMAP experiments. We evaluate the direct detection scattering cross section $\sigma_{\rm SI}$ with the resulting constrained parameters for different LIP masses m_H and investigate the regions in $\sigma_{\rm SI}$–m_H plane that satisfy the bounds from experiments like LUX, XENON etc. We also calculate the signal strength $R_{\gamma\gamma}$ for $h_1 \to \gamma\gamma$ channel in the present framework and compare them with the experimentally obtained limits for this quantity from CMS and ATLAS experiments. This will further constrain the model parameter space. We thus obtain regions in $\sigma_{\rm SI}$–m_H plane in the present framework that satisfy not only the experimental results for dark matter relic density and scattering cross sections but compatible with LHC results too.

The paper is organized as follows. In Sect. 2 we present a description of the model and model parameters with relevant bounds from theory (vacuum stability, perturbativity, and unitarity) and experiments (PLANCK/WMAP, direct detection experiments, LHC etc.). In Sect. 3 we describe the relic density, annihilation cross section measurements for dark matter and modified $R_{\gamma\gamma}$ and $R_{\gamma Z}$ processes due to inert charged scalars. We constrain the model parameter space satisfying the relic density requirements of dark matter and present the correlation between $R_{\gamma\gamma}$ and $R_{\gamma Z}$ processes in Sect. 4. In Sect. 5, we further constrain the results by direct detection bounds on dark matter. Finally, in Sect. 6 we summarize the work briefly with concluding remarks.

2 The model

2.1 Scalar sector

In our model we add an additional SU(2) scalar doublet and a real scalar singlet S to the SM of particle physics. Similar to the widely studied inert doublet model or IDM where the added SU(2) scalar doublet to the SM Lagrangian is made "inert" (by imposing a Z_2 symmetry that ensures no interaction of SM fermions with the inert doublet does not generate any VEV), here too the extra doublet is assumed to be odd under a discrete Z_2 symmetry. Under this Z_2 symmetry, however, all SM particles as also the added singlet S remain unchanged. The potential is expressed as

$$\begin{aligned} V &= m_{11}^2 {\Phi_1}^\dagger \Phi_1 + m_{22}^2 {\Phi_2}^\dagger \Phi_2 + \frac{1}{2} m_s^2 S^2 + \lambda_1 ({\Phi_1}^\dagger \Phi_1)^2 \\ &\quad + \lambda_2 ({\Phi_2}^\dagger \Phi_2)^2 + \lambda_3 (\Phi_1^\dagger \Phi_1)(\Phi_2^\dagger \Phi_2) \\ &\quad + \lambda_4 (\Phi_2^\dagger \Phi_1)(\Phi_1^\dagger \Phi_2) + \frac{1}{2}\lambda_5 [(\Phi_2^\dagger \Phi_1)^2 + (\Phi_1^\dagger \Phi_2)^2] \\ &\quad + \rho_1 (\Phi_1^\dagger \Phi_1) S + \rho_1' (\Phi_2^\dagger \Phi_2) S \\ &\quad + \rho_2 S^2 (\Phi_1^\dagger \Phi_1) + \rho_2' S^2 (\Phi_2^\dagger \Phi_2) + \frac{1}{3}\rho_3 S^3 + \frac{1}{4}\rho_4 S^4, \end{aligned} \tag{1}$$

where $m_k (k = 11, 22, s$ etc.) and all the coupling parameters $(\lambda_i, \rho_i, \rho'_i, i = 1, 2, 3, \ldots,$ etc.) are assumed to be real. In Eq. 1, Φ_1 is the ordinary SM Higgs doublet and Φ_2 is the inert Higgs doublet. After spontaneous symmetry breaking Φ_1 and S acquire VEV such that

$$\Phi_1 = \begin{pmatrix} 0 \\ \frac{1}{\sqrt{2}}(v+h) \end{pmatrix}, \quad \Phi_2 = \begin{pmatrix} H^+ \\ \frac{1}{\sqrt{2}}(H + iA) \end{pmatrix}, \quad S = v_s + s. \tag{2}$$

In the above v_s denotes the VEV of the field S and s is the real singlet scalar. Relations among model parameters can be obtained from the extremum conditions of the potential expressed in Eq. 1 and are given as

$$\begin{aligned} &m_{11}^2 + \lambda_1 v^2 + \rho_1 v_s + \rho_2 v_s^2 = 0, \\ &m_s^2 + \rho_3 v_s + \rho_4 v_s^2 + \frac{\rho_1 v^2}{2 v_s} + \rho_2 v^2 = 0. \end{aligned}$$

Mass terms of various scalar particles as derived from the potential are

$$\begin{aligned} \mu_h^2 &= 2\lambda_1 v^2 \\ \mu_s^2 &= \rho_3 v_s + 2\rho_4 v_s^2 - \frac{\rho_1 v^2}{2 v_s} \\ \mu_{hs}^2 &= (\rho_1 + 2\rho_2 v_s) v \\ m_{H^\pm}^2 &= m_{22}^2 + \lambda_3 \frac{v^2}{2} + \rho_1' v_s + \rho_2' v_s^2 \\ m_H^2 &= m_{22}^2 + (\lambda_3 + \lambda_4 + \lambda_5) \frac{v^2}{2} + \rho_1' v_s + \rho_2' v_s^2 \\ m_A^2 &= m_{22}^2 + (\lambda_3 + \lambda_4 - \lambda_5) \frac{v^2}{2} + \rho_1' v_s + \rho_2' v_s^2. \end{aligned} \tag{3}$$

The mass eigenstates h_1 and h_2 are linear combinations of h and s and can be written as

$$\begin{aligned} h_1 &= h \cos\alpha - s \sin\alpha, \\ h_2 &= h \sin\alpha + s \cos\alpha, \end{aligned} \tag{4}$$

α being the mixing angle between h_1 and h_2, is given by

$$\tan\alpha \equiv \frac{x}{1 + \sqrt{1 + x^2}}, \tag{5}$$

where $x = \frac{2\mu_{hs}^2}{(\mu_h^2 - \mu_s^2)}$. Masses of the physical neutral scalars h_1 and h_2 are

$$m_{1,2}^2 = \frac{\mu_h^2 + \mu_s^2}{2} \pm \frac{\mu_h^2 - \mu_s^2}{2}\sqrt{1 + x^2}. \tag{6}$$

We consider h_1 with mass $m_1 = 125$ GeV as the SM-like Higgs boson and the mass of the other scalar h_2 in the model is denoted as m_2 with $m_2 > m_1$. Couplings of the physical scalars h_1 and h_2 with SM particles are modified by the factors $\cos\alpha$ and $\sin\alpha$, respectively. To ensure that h_1 is the SM-like Higgs, we constrain the mixing angle by imposing the condition $0 \leq \alpha \leq \pi/4$ [24,26]. The coupling λ_5 serves as a mass splitting factor between H and A. We consider H to be the lightest inert particle (LIP) which is stable and is the DM candidate in this work. We take $\lambda_5 < 0$ in order to make H to be the lightest stable inert particle. It is to be noted that for very small mixing, i.e., in the decoupling limit, the present model will be exactly identical to IDM providing a low mass DM ($m_H \leq 80$ GeV) and a high mass DM candidate ($m_H \geq 500$ GeV). In the present framework, the two scalars h_1 and h_2 couple with the lightest inert particle H. Couplings of the scalar bosons (h_1 and h_2) with the inert dark matter H are given by

$$\begin{aligned} \lambda_{h_1 HH} v &= \left(\frac{\lambda_{345}}{2} c_\alpha - \frac{\lambda_s}{2} s_\alpha\right) v, \\ \lambda_{h_2 HH} v &= \left(\frac{\lambda_{345}}{2} s_\alpha + \frac{\lambda_s}{2} c_\alpha\right) v \end{aligned} \tag{7}$$

where $\lambda_{345} = \lambda_3 + \lambda_4 + \lambda_5$, $\lambda_s = \frac{\rho_1' + 2\rho_2' v_s}{v}$ and $s_\alpha (c_\alpha)$ denotes $\sin\alpha (\cos\alpha)$. Couplings of scalar bosons with charged scalars $H^\pm$ are

$$\begin{aligned} \lambda_{h_1 H^+ H^-} v &= (\lambda_3 c_\alpha - \lambda_s s_\alpha)\, v, \\ \lambda_{h_2 H^+ H^-} v &= (\lambda_3 s_\alpha + \lambda_s c_\alpha)\, v. \end{aligned} \tag{8}$$

2.2 Constraints

The model parameters are bounded by theoretical and experimental constraints.

- *Vacuum stability* Vacuum stability constraints require the potential to remain bounded from below. The conditions for the stability of the vacuum are [49,50]

$$\begin{aligned}
&\lambda_1, \lambda_2, \rho_4 > 0, \quad \lambda_3 + 2\sqrt{\lambda_1\lambda_2} > 0,\\
&\lambda_3 + \lambda_4 - |\lambda_5| + 2\sqrt{\lambda_1\lambda_2} > 0,\\
&\rho_2 + \sqrt{\lambda_1\rho_4} > 0, \quad \rho_2' + \sqrt{\lambda_2\rho_4} > 0,\\
&2\rho_2\sqrt{\lambda_2} + 2\rho_2'\sqrt{\lambda_1} + \lambda_3\sqrt{\rho_4}\\
&\quad +2\left(\sqrt{\lambda_1\lambda_2\rho_4} + \sqrt{\left(\lambda_3 + 2\sqrt{\lambda_1\lambda_2}\right)\left(\rho_2 + \sqrt{\lambda_1\rho_4}\right)\left(\rho_2' + \sqrt{\lambda_2\rho_4}\right)}\right) > 0\\
&2\rho_2\sqrt{\lambda_2} + 2\rho_2'\sqrt{\lambda_1} + (\lambda_3 + \lambda_4 - \lambda_5)\sqrt{\rho_4}\\
&\quad +2\left(\sqrt{\lambda_1\lambda_2\rho_4} + \sqrt{\left(\lambda_3 + \lambda_4 - \lambda_5 + 2\sqrt{\lambda_1\lambda_2}\right)\left(\rho_2 + \sqrt{\lambda_1\rho_4}\right)\left(\rho_2' + \sqrt{\lambda_2\rho_4}\right)}\right) > 0. \qquad (9)
\end{aligned}$$

- *Perturbativity* For a theory to be acceptable in perturbative limits, we have to constrain the high energy quartic interactions at tree level. The eigenvalues $|\Lambda_i|$ of quartic couplings (scattering) matrix must be smaller than 4π.
- *LEP* LEP [51] results constrain the Z boson decay width and masses of the scalar particles,

$$\begin{aligned}
&m_H + m_A > m_Z,\\
&m_{H^\pm} > 79.3 \text{ GeV}. \qquad (10)
\end{aligned}$$

- *Relic density* The parameter space is also constrained by the experimental measurement of relic density (WMAP, PLANCK etc.) of dark matter candidate. The relic density of the lightest inert particle (LIP) serving as a viable candidate for dark matter in the present model must satisfy the PLANCK results,

$$\Omega_{\rm DM}h^2 = 0.1199 \pm 0.0027. \qquad (11)$$

- *Higgs to diphoton rate* $R_{\gamma\gamma}$ A bound on the Higgs to two photon channel has been obtained from experiments performed by LHC. The measured signal strength for the Higgs to diphoton channel obtained from ATLAS at 95 % CL is

$$R_{\gamma\gamma}|_{\rm ATLAS} = 1.57^{+0.33}_{-0.29},$$

whereas the best fit value of $R_{\gamma\gamma}$ for a 125 GeV Higgs with 3.2σ excess in local significance corresponding to an expected value of 4.2σ measured by CMS is

$$R_{\gamma\gamma}|_{\rm CMS} = 0.78^{+0.28}_{-0.26}.$$

- *Direct detection experiments* The bounds on dark matter from direct detection experiments are based on the elastic scattering of the dark matter particle off a scattering nucleus. Dark matter direct detection experiments set constraints on the dark matter-nucleus (nucleon) elastic scattering cross section. Limits on scattering cross sections for different dark matter mass cause further restrictions on the model parameters. Experiments like CDMS, DAMA, CoGeNT, CRESST etc. provide effective bounds on low mass dark matter. Stringent bounds on medium mass and high mass dark matter are obtained from XENON100 and LUX experiments.

3 Dark matter

3.1 Relic density

The relic density of dark matter is constrained by the results of PLANCK and WMAP. The dark matter relic abundance for the model is evaluated by solving the evolution of Boltzmann equation given as [52]

$$\frac{{\rm d}n_H}{{\rm d}t} + 3{\rm H}n_H = -\langle\sigma{\rm v}\rangle(n_H^2 - n_{H\rm eq}^2). \qquad (12)$$

In Eq. 12, $n_H(n_{H_{\rm eq}})$ denotes the number density (equilibrium number density) of dark matter H and H is the Hubble constant. In Eq. 12, $\langle\sigma{\rm v}\rangle$ denotes the thermal averaged annihilation cross section of dark matter particle to SM species. The dark matter relic density can be obtained by solving Eq. 12 and is obtained as

$$\Omega_{\rm DM}{\rm h}^2 = \frac{1.07\times10^9 x_F}{\sqrt{g_*}M_{\rm Pl}\langle\sigma{\rm v}\rangle}. \qquad (13)$$

In the above, $M_{\rm Pl} = 1.22\times10^{19}$ GeV is the Planck scale mass whereas g_* is the effective number of degrees of freedom in

thermal equilibrium and h is the Hubble parameter in units of 100 km s^{-1} Mpc^{-1}. In Eq. 13, $x_F = M/T_F$, where T_F is the freeze out temperature of the annihilating particle and M is the mass of the dark matter (m_H for the present scenario). The freeze out temperature T_F for the dark matter is obtained from the iterative solution to the equation

$$x_F = \ln\left(\frac{M}{2\pi^3}\sqrt{\frac{45M_{\rm Pl}^2}{2g_* x_F}}\langle\sigma \mathrm{v}\rangle\right). \tag{14}$$

3.2 Annihilation cross section

Annihilation of inert dark matter H to SM particles is governed by processes involving scalar (h_1, h_2) mediated s($\simeq 4m_H^2$) channels. Thermal averaged annihilation cross sections $\langle\sigma \mathrm{v}\rangle$ of dark matter H to SM fermions are given as

$$\langle\sigma \mathrm{v}_{HH\to f\bar{f}}\rangle = n_c\frac{m_f^2}{\pi}\beta_f^3\left|\frac{\lambda_{h_1HH}\cos\alpha}{4m_H^2 - m_1^2 + i\Gamma_1 m_1} + \frac{\lambda_{h_2HH}\sin\alpha}{4m_H^2 - m_2^2 + i\Gamma_2 m_2}\right|^2. \tag{15}$$

In the above, m_x represents the mass of the particle $x(\equiv f,\ H$ etc.), n_c is the color quantum number (3 for quarks and 1 for leptons) with $\beta_a = \sqrt{1-\frac{m_a^2}{m_H^2}}$ and $\Gamma_i (i = 1, 2)$ denotes the total decay width of each of the two scalars h_1 and h_2. For DM mass $m_H > (m_W, m_Z)$, the channels of annihilation of DM to gauge boson (W or Z) will yield a high annihilation cross section. Since $\Omega_{\rm DM} \sim \langle\sigma \mathrm{v}\rangle^{-1}$ (Eq. 13), the relic density for the dark matter with mass $m_H > m_W$ or m_Z in the present model in fact falls below the relic density given by WMAP or PLANCK as the four point interaction channel $HH \to W^+W^-$ or ZZ will be accessible and as a result an increase in the total annihilation cross section will be observed. Thus the possibility of a single component DM in the present framework is excluded for mass $m_H > m_W,\ m_Z$.[1] The invisible decay of $h_i (i = 1, 2)$ depends on the DM mass m_H and is kinematically forbidden for $m_H > m_i/2\ (i = 1, 2)$. The contributions of the invisible decay widths for h_1 and h_2 are taken into account when the condition $m_H < m_i/2\ (i = 1, 2)$ is satisfied. The invisible decay width is represented by the relation

$$\Gamma_i^{\rm inv}(h_i \to 2H) = \frac{\lambda_{h_iHH}^2 v^2}{16\pi m_i}\sqrt{1-\frac{4m_H^2}{m_i^2}}. \tag{16}$$

[1] Similar results for IDM are also obtained in a previous work (Ref. [53]), where two component dark matter was considered in order to circumvent this problem.

3.3 Modification of $R_{\gamma\gamma}$ and $R_{\gamma Z}$

Recent studies of IDM [54–56] and two Higgs doublet models [57,58] have reported that a low mass charged scalar could possibly enhance the $h_1 \to \gamma\gamma$ signal strength $R_{\gamma\gamma}$. The correlation of $R_{\gamma\gamma}$ with $R_{\gamma Z}$ is also accounted for as well [55,58]. The quantities $R_{\gamma\gamma}$ and $R_{\gamma Z}$ are expressed as

$$R_{\gamma\gamma} = \frac{\sigma(pp\to h_1)}{\sigma(pp\to h)^{\rm SM}}\frac{Br(h_1\to\gamma\gamma)}{Br(h\to\gamma\gamma)^{\rm SM}} \tag{17}$$

$$R_{\gamma Z} = \frac{\sigma(pp\to h_1)}{\sigma(pp\to h)^{\rm SM}}\frac{Br(h_1\to\gamma Z)}{Br(h\to\gamma Z)^{\rm SM}}, \tag{18}$$

where σ is the Higgs production cross section and Br represents the branching ratio of Higgs to final states. The branching ratio to any final state is given by the ratio of partial decay width for the particular channel to the total decay width of decaying particle. For IDM with additional singlet scalar, the ratio $\frac{\sigma(pp\to h_1)}{\sigma(pp\to h)^{\rm SM}}$ in Eqs. 17–18 is represented by a factor $\cos^2\alpha$. Standard Model branching ratios $Br(h\to\gamma\gamma)^{\rm SM}$ and $Br(h\to\gamma Z)^{\rm SM}$ for a 125 GeV Higgs boson is 2.28×10^{-3} and 1.54×10^{-3}, respectively [59]. To evaluate the branching ratios $Br(h_1\to\gamma\gamma)$ and $Br(h_1\to\gamma Z)$, we compute the total decay width of h_1. The invisible decay of h_1 to the dark matter particle H is also taken into account and evaluated using Eq. 16 when the condition $m_H < m_1/2$ is satisfied. Partial decay widths $\Gamma(h_1\to\gamma\gamma)$ and $\Gamma(h_1\to\gamma Z)$ according to the model are given by

$$\Gamma(h_1\to\gamma\gamma) = \frac{G_F\alpha_s^2 m_1^3}{128\sqrt{2}\pi^3}\left|\cos\alpha\left(\frac{4}{3}F_{1/2}\left(\frac{4m_t^2}{m_1^2}\right) + F_1\left(\frac{4m_W^2}{m_1^2}\right)\right) + \frac{\lambda_{h_1H^+H^-}v^2}{2m_{H^\pm}^2}F_0\left(\frac{4m_{H^\pm}^2}{m_1^2}\right)\right|^2,$$

$$\Gamma(h_1\to\gamma Z) = \frac{G_F^2\alpha_s}{64\pi^4}m_W^2 m_1^3\left(1-\frac{m_Z^2}{m_1^2}\right)^3 \times\left|-2\cos\alpha\frac{1-\frac{8}{3}s_W^2}{c_W}F'_{1/2}\left(\frac{4m_t^2}{m_1^2},\frac{4m_t^2}{m_Z^2}\right) - \cos\alpha F'_1\left(\frac{4m_W^2}{m_1^2},\frac{4m_W^2}{m_Z^2}\right) + \frac{\lambda_{h_1H^+H^-}v^2}{2m_{H^\pm}^2}\frac{(1-2s_W^2)}{c_W}I_1\left(\frac{4m_{H^\pm}^2}{m_1^2},\frac{4m_{H^\pm}^2}{m_Z^2}\right)\right|^2, \tag{19}$$

where G_F is the Fermi constant, m_x denotes the mass of particle $x(x \equiv 1, W, Z, t, H^\pm)$ etc. and $s_W(c_W)$ represents $\sin\theta_W(\cos\theta_W)$, θ_W being the Weinberg mixing angle. The expressions for various loop factors ($F_{1/2}$, F_1, F_0, $F'_{1/2}$, F'_1 and I_1) appearing in Eq. 19 are given in Appendix. It is to be noted that a similar derivation of decay widths and signal strengths ($R'_{\gamma\gamma}$ or $R'_{\gamma Z}$) for the other scalar

h_2 can be obtained by replacing $m_1, \cos\alpha, \lambda_{h_1H^+H^-}$ with $m_2, \sin\alpha, \lambda_{h_2H^+H^-}$, respectively, and this is addressed in Sect. 5.

4 Analysis of $R_{\gamma\gamma}$ and $R_{\gamma Z}$

In this section we compute the quantities $R_{\gamma\gamma}$ and $R_{\gamma Z}$ in the framework of the present model. We restrict the allowed model parameter space for our analysis using the vacuum stability, perturbative unitarity, LEP bounds along with the relic density constraints described in Sect. 2.2. Dark matter relic density is evaluated by solving the Boltzmann equation presented in Sect. 3.1 with the expression for annihilation cross section given in Eq. 15. Model parameters (λ_i, ρ_i), should remain small in order to satisfy perturbative bounds and relic density constraints. Calculations are made for the model parameter limits given below,

$$\begin{aligned}
&m_1 = 125\ \text{GeV},\\
&80\ \text{GeV} \le m_{H^\pm} \le 400\ \text{GeV},\\
&0 < m_H < m_{H^\pm},\ m_A,\\
&0 < \alpha < \pi/4,\\
&-1 \le \lambda_3 \le 1,\\
&-1 \le \lambda_{345} \le 1,\\
&-1 \le \lambda_s \le 1.
\end{aligned} \tag{20}$$

The enhancement of Higgs to diphoton signal depends on the contribution from the charged scalar loop (Eq. 19). Since for higher value of the charged scalar mass $(m_{H^\pm})$, the contribution from the charged scalar loop will reduce, we expect mass of the charged scalar to be small. Due to this reason, we kept charged scalar mass to be less than 400 GeV. As mentioned earlier, due to large DM annihilation cross section to W or Z boson channel, high mass DM in the present scenario will fail to satisfy DM relic abundance unless we assume a TeV scale dark matter [60]. Hence, for the range considered for the charged scalar mass, possibility of having a high mass DM regime in decoupling limit ($\alpha \to 0$) is excluded and we explore the low mass region only where enhancement is significant. The couplings λ_{h_1HH} and λ_{h_2HH} (Eq. 7) are required to calculate the scattering cross section of the dark matter off a target nucleon. Dark matter direct detection experiments are based on these scattering processes whereby the recoil energy of the scattered nucleon is measured. Thus the couplings λ_{h_1HH} and λ_{h_2HH} can be constrained by comparing the computed values of the scattering cross section for different dark matter masses with those given by different dark matter direct detection experiments. In the present work, $|\lambda_{h_1HH}, \lambda_{h_2HH}| \le 1$ is adopted. The following bounds on the parameters will also constrain the couplings $\lambda_{h_1H^+H^-}$ and $\lambda_{h_2H^+H^-}$ (Eq. 8). Using Eqs. 12–16 we scan over the parameter space mentioned in Eq. 20 where we also impose the conditions $|\lambda_{h_1H^+H^-},\ \lambda_{h_2H^+H^-}| \le 2$ to calculate $R_{\gamma\gamma,\ \gamma Z}$ in the present model. Comparing the experimentally observed dark matter relic density with the calculated value restricts the allowed model parameter space and gives the range of mass that satisfies observed DM relic density. We have made our calculations for two different values of the singlet scalar (h_2) mass, namely $m_2 = 150$ and 300 GeV. Scanning of the full parameter space yields the result that, for all the cases considered, the limits $|\lambda_{h_1HH}, \lambda_{h_2HH}| \le 0.7$ are required for satisfying observed DM relic abundance. Our calculation reveals that $|\lambda_{h_1H^+H^-}, \lambda_{h_2H^+H^-}| \le 1.5$ are needed in order to satisfy the observed relic density of dark matter. Using the allowed parameter space thus obtained, we calculate the signal strengths $R_{\gamma\gamma}$ and $R_{\gamma Z}$ (Eqs. 17–18) by evaluating the corresponding decay widths given in Eq. 19.

In Fig. 1a, b shown are the regions in the $R_{\gamma\gamma}$–m_H plane for the parameter values that satisfy the DM relic abundance. As mentioned earlier, results are presented for two values of the h_2 mass, namely 150 and 300 GeV. Since for the low mass DM region, the invisible decay channel of h_1 to DM pair remains open, enhancement of $R_{\gamma\gamma}$ is not possible in this regime. $R_{\gamma\gamma}$ becomes greater than unity near the region of resonance where $m_H \approx m_2/2$ for $m_2 = 150$ GeV. The

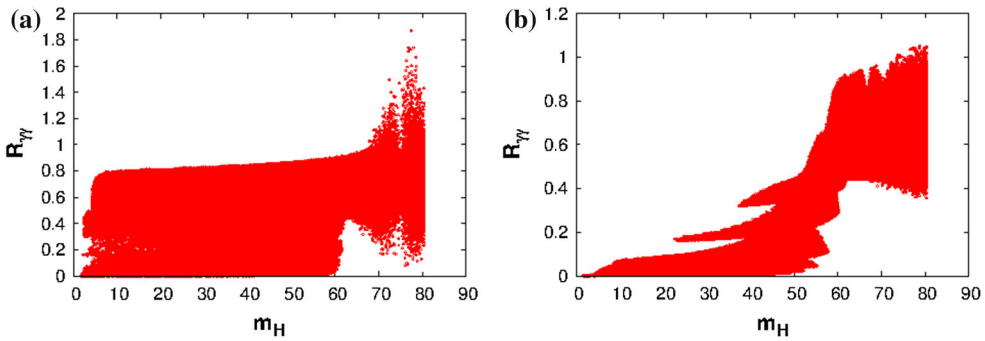

Fig. 1 Variation of $R_{\gamma\gamma}$ with DM mass m_H satisfying DM relic density for $m_2 = 150$ and 300 GeV

resonant enhancement is more pronounced for lighter $m_{H^\pm}$ mass. However, no such resonant enhancement is obtained for $m_2 = 300$ GeV but a small enhancement occurs near $m_H \simeq 80$ GeV for a light charged scalar ($m_{H^\pm} \leq 100$ GeV). The region that describes the $R_{\gamma\gamma}$ enhancement is reduced with increasing h_2 mass and thus enhancement is not favored for higher values of the h_2 mass. For the rest of the allowed DM mass parameter space, $R_{\gamma\gamma}$ remains less than 1 and decreases with higher values of the h_2 mass. The results presented in Fig. 1 indicate that the observed enhancement of the $h_1 \to \gamma\gamma$ signal could be a possible indication of the presence of h_2 since $R_{\gamma\gamma} \gtrsim 1$ occurs near the resonance of h_2, which contributes to the total annihilation cross section measured via Eq. 15. The $R_{\gamma\gamma}$ value depends on the coupling $\lambda_{h_1 H^+ H^-}$ and becomes greater than unity only for $\lambda_{h_1 H^+ H^-} < 0$ and interferes constructively with the other loop contributions. Technically, $R_{\gamma\gamma}$ depends on the values of the h_2 mass, charged scalar mass $m_{H^\pm}$, coupling $\lambda_{h_1 H^+ H^-}$, and the decay width of invisible decay channel $\Gamma_{\rm inv}(h_1 \to HH)$. A similar variation for the $h_1 \to \gamma Z$ channel (computed using Eqs. 18, 19 and 20) yields a smaller enhancement for $R_{\gamma Z}$ in comparison with $R_{\gamma\gamma}$. This phenomenon can also be verified from the correlation between $R_{\gamma\gamma}$ and $R_{\gamma Z}$. The correlations between the signals $R_{\gamma\gamma}$ and $R_{\gamma Z}$ are shown in Fig. 2a, b for $m_2 = 150, 300$ GeV, respectively. Variations of $R_{\gamma\gamma}$ and $R_{\gamma Z}$ satisfy all necessary parameter constraints including the relic density requirements for DM. Figure 2 also indicates that, with the increase in the mass (m_2) of h_2, the enhancements of $R_{\gamma\gamma}$ and $R_{\gamma Z}$ are likely to reduce. For $m_2 = 150$ GeV, $R_{\gamma\gamma}$ enhances up to two times whereas $R_{\gamma Z}$ increases nearly by a factor 1.2 with respect to the corresponding values predicted by SM. On the other hand, for $m_2 = 300$ GeV, $R_{\gamma\gamma}$ varies linearly with $R_{\gamma Z}$ ($R_{\gamma\gamma} \simeq R_{\gamma Z}$) without any significant enhancement. For low mass dark matter ($m_H \lesssim m_1/2$), invisible decay channel of h_1 remains open and the processes $h_1 \to \gamma\gamma$ and $h_1 \to \gamma Z$ suffer from considerable suppressions. These result in the correlation between the channels $h_1 \to \gamma\gamma$ and $h_1 \to \gamma Z$, which appear to become stronger, and the $R_{\gamma\gamma}$ vs. $R_{\gamma Z}$ plot shows more linearity with increasing h_2 mass. For larger h_2 masses, the corresponding charged scalar ($H^\pm$) masses for which $R_{\gamma\gamma,\gamma Z} > 1$ tends to increase. Since any increase in the $H^\pm$ mass will affect the contribution from the charged scalar loop, the decay widths $\Gamma(h_1 \to \gamma\gamma, \gamma Z)$ or signal strengths $R_{\gamma\gamma,\gamma Z}$ are likely to reduce. Our numerical results exhibit a positive correlation between the signal strengths $R_{\gamma\gamma}$ and $R_{\gamma Z}$. This is an important feature of the model. Since signal strengths tend to increase with relatively smaller values of m_2, the possibility of having a light singlet like scalar is not excluded. The coupling of h_2 with the SM sector is suppressed by a factor $\sin\alpha$, which results in a decrease in the signal strengths from h_2 and makes their observations difficult.

5 Direct detection

In this section we further investigate whether the allowed model parameter space (and enhancement of $R_{\gamma\gamma,\gamma Z}$) is consistent with dark matter direct search experiments. Within the framework of our model and allowed values of parameter region obtained in Sect. 4, we calculate the spin-independent (SI) elastic scattering cross section for the dark matter candidate in our model off a nucleon in the detector material. We then compare our results with those given by various direct detection experiments and examine the plausibility of our model in explaining the direct detection experimental results. The DM candidate in the present model interacts with the SM via processes led by Higgs exchange. The spin-independent elastic scattering cross section $\sigma_{\rm SI}$ is of the form

$$\sigma_{\rm SI} \simeq \frac{m_r^2}{\pi}\left(\frac{m_N}{m_H}\right)^2 f^2 \left(\frac{\lambda_{h_1 HH}\cos\alpha}{m_1^2} + \frac{\lambda_{h_2 HH}\sin\alpha}{m_2^2}\right)^2, \tag{21}$$

where m_N and m_H are the masses of scattered nucleon and DM, respectively, f represents the scattering factor

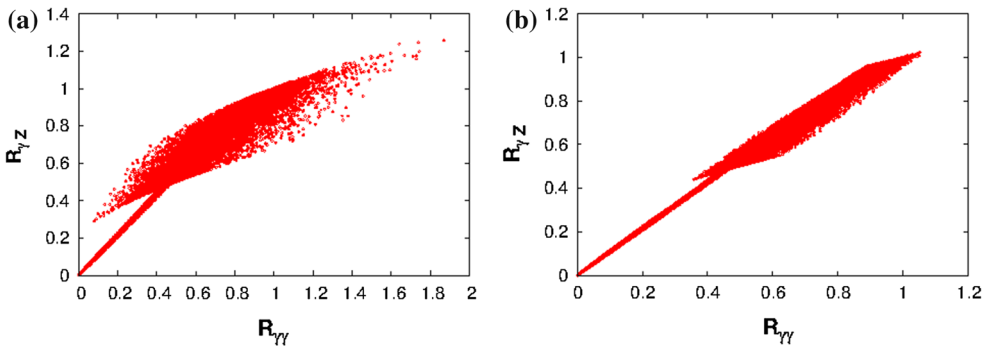

Fig. 2 Correlation plots between $R_{\gamma\gamma}$ and $R_{\gamma Z}$ for two choices of the h_2 mass (150 and 300 GeV)

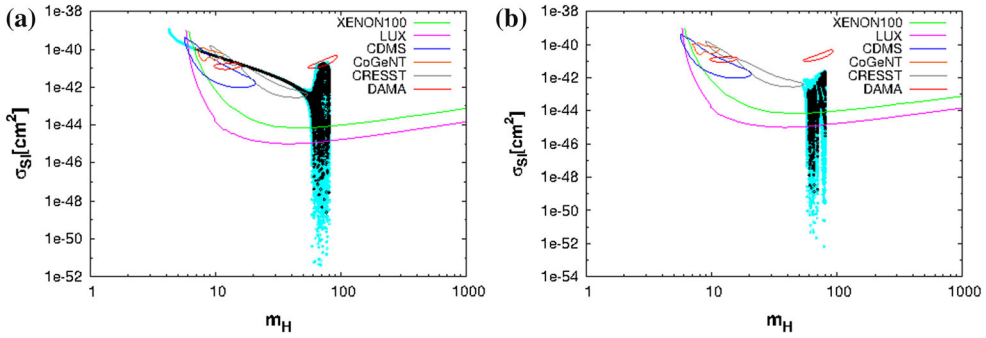

Fig. 3 Allowed regions in m_H–σ_{SI} plane for $m_2 = 150$ and 300 GeV

that depends on the pion–nucleon cross section and quarks involved in the process and $m_r = \frac{m_N m_H}{m_N + m_H}$ is the reduced mass. In the present framework $f = 0.3$ [61] is considered. The computations of $\sigma_{\rm SI}$ for the dark matter candidate in the present model are carried out with those values of the couplings restricted by the experimental value of relic density. In Fig. 3a, b, we present the variation of elastic scattering cross section calculated using Eq. 21, with LIP dark matter mass (m_H) for two values of the h_2 masses $m_2 = 150$ and 300 GeV satisfying the CMS limit of $R_{\gamma\gamma}$. We assume h_1 to be SM-like Higgs and restrict the mixing angle α such that the condition $\cos\alpha \gtrsim 1/\sqrt{2}$ is satisfied. In each of the $\sigma_{\rm SI}$–m_H plots of Fig. 3a, b the light blue region satisfies the CMS limit of $R_{\gamma\gamma}$ for two chosen values of m_2. Also marked in black are the specific zones that correspond to the central value of $R_{\gamma\gamma}|_{\rm CMS} = 0.78$. The bounds on the $\sigma_{\rm SI}$-DM mass obtained from DM direct search experiments such as XENON100, LUX, CDMS, CoGeNT, CRESST are shown in Fig. 3a, b, superimposed on the computed results for comparison. From Fig. 3a, b one notes that for the case of $m_2 = 150$ GeV, the DM candidate in our model partly satisfies the bounds obtained from low mass dark matter direct detection experiments like CoGeNT, CDMS, CRESST, DAMA but are disfavored for $m_2 = 300$ GeV. It is therefore evident from Fig. 3a, b that imposition of the signal strength ($R_{\gamma\gamma}$) results obtained from LHC further constrains the allowed scattering cross section limits obtained from direct detection experimental results for the DM candidate in our model. Investigating the region allowed by LUX and XENON100 experiments along with other direct dark matter experiments such as CDMS etc., it is evident from Fig. 3a, b that our model suggests a DM candidate within the range $m_H = 60$–80 GeV with scattering cross section values $\sim 10^{-45}$–10^{-49} cm^2 with $m_1 = 125$ GeV, which is an SM-like scalar. There is, however, little negligibly small allowed parameter space with $\sigma_{\rm SI}$ below $\sim 10^{-49}$ cm^2. Hence, in the present model H can serve as a potential dark matter candidate and future experiments with higher sensitivity like XENON1T [62], SuperCDMS [63] etc. are expected to constrain or rule out the viability of this model. A similar procedure has been adopted for restricting the $\sigma_{\rm SI}$–m_H space using $R_{\gamma\gamma}$ limits from ATLAS experiment. We found that the region of the DM parameter space for the case of the Higgs to diphoton signal strength predicted by ATLAS with 95 % CL is completely ruled out as the allowed DM mass region in the model (for both $m_2 = 150$ and 300 GeV) cannot satisfy the latest direct detection bounds from XENON100 and LUX experiments. In the present model we so far adopt the consideration that h_1 plays the role of SM Higgs and hence in our discussion we consider $h_1 \to \gamma\gamma$ for constraining our parameter space. The model considered in this work also provides us with a second scalar, namely h_2. Since LHC has not yet observed a second scalar, it is likely that the other scalar h_2 is very weakly coupled to SM sector so that the corresponding branching ratios (signal strengths) are small. Also significant enhancement of the process $h_2 \to \gamma\gamma$ can occur due to the presence of charge scalar ($H^{\pm}$). Hence, in the present scenario we require the $h_2 \to \gamma\gamma$ branching ratio or signal strength ($R'_{\gamma\gamma}$) to be very small compared to that for h_1. Needless to mention that the couplings required to compute $R_{\gamma\gamma}$ and $R'_{\gamma\gamma}$ are restricted by dark matter constraints. We address these issues by computing $R'_{\gamma\gamma}$ values and comparing them with $R_{\gamma\gamma}$.[2] The computations of $R_{\gamma\gamma}$ and $R'_{\gamma\gamma}$ initially involve the dark matter model parameter space that yields the dark matter relic density in agreement with PLANCK data as also the stringent direct detection cross section bound obtained from LUX. $R_{\gamma\gamma}$ values thus obtained are not found to satisfy the experimental range given by ATLAS experiment. The resulting $R_{\gamma\gamma} - R'_{\gamma\gamma}$ is further restricted for those values of $R_{\gamma\gamma}$ which are within the limit of $R_{\gamma\gamma}|_{\rm CMS}$ given by CMS experiment. The region with green scattered points in Fig. 4a, b corresponds to the $R_{\gamma\gamma}$–$R'_{\gamma\gamma}$ space consistent with the model parameters that are allowed by DM relic density obtained from PLANCK, direct detection experiment bound from LUX and $R_{\gamma\gamma}|_{\rm CMS}$ for $m_2 = 150$ and 300 GeV. It is to

[2] Since $R'_{\gamma\gamma}$ and $R'_{\gamma Z}$ are correlated, any suppression in $h_2 \to \gamma\gamma$ will be followed by similar effects in $h_2 \to \gamma Z$.

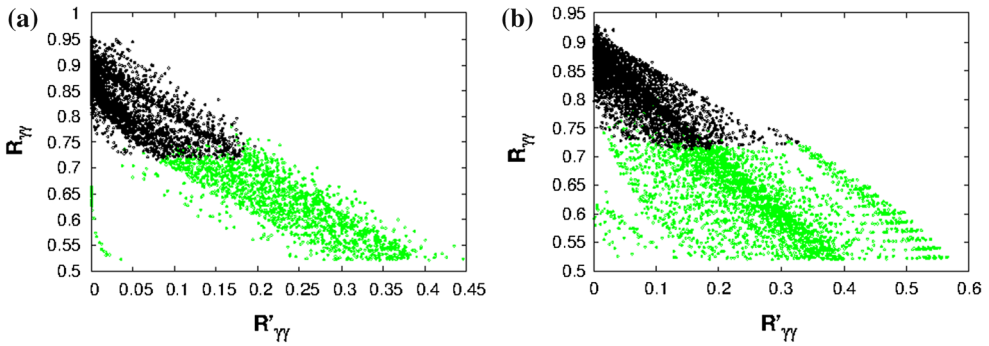

Fig. 4 Allowed regions in $R_{\gamma\gamma}$–$R'_{\gamma\gamma}$ plane for $m_2 = 150$ and 300 GeV

be noted that $R_{\gamma\gamma}$ is not the only constraint obtained from LHC experiments, we have to consider other decay channels of h_1 as well. In the present model, signal strengths (R_1) of h_1 to any particular decay channel (excluding $\gamma\gamma$ and γZ channel) can be expressed as

$$R_1 = c_\alpha^4 \frac{\Gamma_1^{\rm SM}}{\Gamma_1} \tag{22}$$

where $\Gamma_1^{\rm SM}$ represents the total SM decay width of h_1, Γ_1 denotes the total decay width of h_1 in the present model. Since contributions of $h_1 \to \gamma\gamma$ and $h_1 \to \gamma Z$ channels to the total decay width are negligibly small, total decay width Γ_1 can be written as

$$\Gamma_1 = c_\alpha^2 \Gamma_1^{\rm SM} + \Gamma_1^{\rm inv} \tag{23}$$

where $\Gamma_1^{\rm inv}$ is the invisible decay width of h_1 as expressed in Eq. 16. Similarly the signal strength of the singlet like scalar h_2 can be given as

$$R_2 = s_\alpha^4 \frac{\Gamma_2^{\rm SM}}{\Gamma_2} \tag{24}$$

with $\Gamma_2 = s_\alpha^2 \Gamma_2^{\rm SM} + \Gamma_2^{\rm inv} + \Gamma_{211}$, where Γ_{211} is the decay width of singlet scalar h_2 to SM Higgs h_1 is given as

$$\Gamma_{211} = \frac{\lambda_{h_2 h_1 h_1}^2}{32\pi m_2} \sqrt{1 - \frac{4m_1^2}{m_2^2}}, \tag{25}$$

with

$$\begin{aligned} \lambda_{h_2 h_1 h_1} = {} & 3\lambda_1 v c_\alpha^2 s_\alpha + \frac{\rho_1}{2}(-2s_\alpha^2 c_\alpha + c_\alpha^3) \\ & + \rho_2 v(-2s_\alpha c_\alpha^2 + s_\alpha^3) + \rho_2 v_s(-2s_\alpha^2 c_\alpha + c_\alpha^3) \\ & + \rho_3 s_\alpha^2 c_\alpha + 3\rho_4 v_s s_\alpha^2 c_\alpha. \end{aligned} \tag{26}$$

In the present work, we constrain the signal strength R_1 in order to invoke h_1 as the SM-like scalar and set $R_1 \geq 0.8$ [64]. In Fig. 4a, b the region shown in black scattered points are in agreement with the condition $R_1 \geq 0.8$. We found that the signal strength R_2 for the other scalar involved remains small ($R_2 \leq 0.2$) and may also suffer appreciable reduction due to the $h_2 \to HH$ channel for $m_H < m_2/2$.

Constraints from the signal strength R_1 along with direct detection bound predicted by LUX restrict the allowed model parameter space with $|\lambda_{h_1 HH}| \leq 0.04$ and $|\lambda_{h_2 HH}| \leq 0.5$ for $m_2 = 300$ GeV and couplings are even smaller for the other scenario when $m_2 = 150$ GeV. Further reduction to the allowed limit of $\lambda_{h_1 HH}$ occurs for DM mass $m_H \leq m_1/2$ satisfying the range $|\lambda_{h_1 HH}| \leq 0.01$, which indicates that invisible decay branching ratio is small. Hence, according to the model, even if we restrict the results with the conditions $R'_{\gamma\gamma} \leq 0.1$ and $R_1 \geq 0.8$ [64] along with the DM relic density obtained from PLANCK and direct detection bounds obtained from LUX ($\sigma_{\rm SI} \leq 10^{-45}$ cm^2), the model still provides a feasible DM candidate with an appreciable range of allowed parameter space. In Table 1 we further demonstrate that within the framework of our proposed model for LIP dark matter, $R'_{\gamma\gamma}$ is indeed small compared to $R_{\gamma\gamma}$. We tabulate the values of both $R_{\gamma\gamma}$ and $R'_{\gamma\gamma}$ for some chosen values of LIP dark matter mass m_H fulfilling the bound obtained from signal strength $R_1 \geq 0.8$ [64]. These numerical values are obtained from the computational results consistent with LUX direct DM search bound. Also in Table 1 are given the corresponding mixing angles α between h_1 and h_2, couplings $\lambda_{h_i HH}$ ($i = 1, 2$), the scalar masses $m_{H^\pm}$, h_2 to diphoton branching ratio, the scattering cross section $\sigma_{\rm SI}$ and invisible branching ratio $Br_{\rm inv}$ of h_1 for two different values of m_2 considered in the work. It is also evident from Table 1 that $R_{\gamma\gamma} >> R'_{\gamma\gamma}$ and the respective mixing angle values are small. In fact, for some cases such as for $m_H = 61.06$ GeV ($m_2 = 150$ GeV) $R_{\gamma\gamma} = 0.875$ whereas $R'_{\gamma\gamma} \sim 10^{-5}$ and α is as small as 6. The coupling $\lambda_{h_1 HH}$ remains small and is responsible for the small invisible decay branching ratio (denoted by $BR_{\rm inv}$ in Table 1) of the SM-like scalar h_1. This demonstrates that the scalar h_1 in Eq. 4 is mostly dominated by the SM-like Higgs component and the major component in the other scalar is the real scalar singlet s of the proposed model.

Table 1 Benchmark points satisfying observed DM relic density obtained from PLANCK data and direct detection cross section reported by LUX results for two different choices of the h_2 mass

m_2 (GeV)	m_H (GeV)	$m_{H^\pm}$ (GeV)	α (deg)	λ_{h_1HH}	λ_{h_2HH}	$R_{\gamma\gamma}$	$R'_{\gamma\gamma}$	$Br(h_2 \to \gamma\gamma)$	$\sigma_{\rm SI}$ in cm^2	$Br_{\rm inv}$
150.00	61.06	125.00	06	−5.5e−03	8.5e−02	0.875	3.59e−05	4.627e−06	5.890e−47	1.51e−02
	67.05	132.00	09	9.0e−03	−8.0e−02	0.874	4.62e−04	2.659e−05	3.745e−48	–
	73.07	171.00	07	−2.0e−03	5.8e−02	0.883	4.79e−04	4.541e−05	7.001e−46	–
300.0	61.72	97.00	01	−2.5e−03	−8.3e−04	0.906	2.93e−04	1.238e−05	7.245e−46	2.31e−02
	64.78	144.50	08	7.0e−03	−0.30	0.876	2.88e−02	1.917e−05	2.290e−47	–
	70.12	117.00	15	−2.0e−02	0.48	0.857	3.35e−03	6.461e−07	4.659e−46	–

6 Summary

In this work we have proposed a model for dark matter where we consider an extended two Higgs doublet model with an additional singlet scalar. The DM candidate follows by considering one of the Higgs doublets to be an inert Higgs doublet. A Z_2 symmetry imposed on the potential ensures the lightest inert particle or LIP dark matter from the added inert doublet is stable. The inert doublet does not generate any VEV and hence cannot couple to the Standard Model fermions directly. The scalar singlet, having no such discrete symmetry, acquires a non-zero VEV and mixes up with the SM Higgs. The unknown couplings of the model, which are basically the model parameters, are restricted with theoretical and experimental bounds. The mixing of the SM Higgs and the singlet scalar gives rise to two scalar states, namely h_1 and h_2. For small mixing, h_1 behaves as the SM Higgs and h_2 as the added scalar. We extensively explored the scalar sector of the model and studied the signal strengths $R_{\gamma\gamma}$ and $R_{\gamma Z}$ for the SM-like Higgs (h_1) in the model. The range and the region of enhancement of $R_{\gamma\gamma}$ depend on the mass of the singlet like scalar h_2. Appreciable enhancements of both $h_1 \to \gamma\gamma$ and $h_1 \to \gamma Z$ signals depend on h_2 mass and occur near the resonance of h_2. An increase in the signal strengths is not allowed for heavier values of the h_2 mass. Enhancement of signals is forbidden when the invisible decay channel remains open. The extent of enhancement depends on the charged scalar mass and this occurs only when the Higgs-charged scalar coupling $\lambda_{h_1H^+H^-} < 0$. We first restrict our parameter space by calculating the relic density of LIP dark matter in the framework of our model. Using the resultant parameter space obtained from the observed relic density bounds we evaluate the signal strengths $R_{\gamma\gamma}$ and $R_{\gamma Z}$ for different dark matter masses. We then restrict the parameter space by calculating the spin-independent scattering cross section and comparing it with the existing limits from ongoing direct detection experiments like CDMS, CoGeNT, DAMA, XENON100, LUX etc. Employing additional constraints by requiring that $R_{\gamma\gamma}$ and $R_{\gamma Z}$ will satisfy the CMS bounds and ATLAS bounds, we see that the present model provides a good and viable DM candidate in the mass region 60–80 GeV, consistent with LUX and XENON100 bounds. We obtain the result that $R_{\gamma\gamma}(>1.0)$ in the present framework does not seem to be favored by LUX and XENON100 data. Therefore, we conclude that in the present framework, the Inert Doublet Model with additional scalar singlet provides a viable DM candidate with a mass range of 60–80 GeV, which not only is consistent with the direct detection experimental bounds and the PLANCK results for the relic density but also is in agreement with the Higgs search results of LHC. A singlet like scalar that couples weakly with the SM Higgs may also exist which could enrich the Higgs sector and may be probed in future collider experiments.

Acknowledgments A.D.B. would like to thank A. Biswas and D. Das for useful discussions.

Appendix

In Sect. 3.3 we have derived the decay widths $h_1 \to \gamma\gamma$ and $h_1 \to \gamma Z$ in terms of the loop factors $F_{1/2}$, F_1, F_0, $F'_{1/2}$, F'_1, and I_1. The expressions of the factors $F_{1/2}$, F_1, F_0 (for the measurement of $h_1 \to \gamma\gamma$ decay width) are given as [65–67]

$$F_{1/2}(\tau) = 2\tau[1 + (1-\tau)f(\tau)],$$
$$F_1(\tau) = -[2 + 3\tau + 3\tau(2-\tau)f(\tau)],$$
$$F_0(\tau) = -\tau[1 - \tau f(\tau)],$$

and

$$f(\tau) = \begin{cases} \arcsin^2\left(\frac{1}{\sqrt{\tau}}\right) & \text{for } \tau \geq 1, \\ -\frac{1}{4}\left[\log\left(\frac{1+\sqrt{1-\tau}}{1-\sqrt{1-\tau}}\right) - i\pi\right]^2 & \text{for } \tau < 1. \end{cases}$$

The loop factors for the decay $h_1 \to \gamma Z$ are adopted from Refs. [65–67] and they are

$$F'_{1/2}(\tau,\lambda) = I_1(\tau,\lambda) - I_2(\tau,\lambda),$$

$$F'_1(\tau,\lambda) = c_W \left\{ 4\left(3 - \frac{s_W^2}{c_W^2}\right) I_2(\tau,\lambda) + \left[\left(1+\frac{2}{\tau}\right)\frac{s_W^2}{c_W^2} - \left(5+\frac{2}{\tau}\right)\right] I_1(\tau,\lambda) \right\},$$

where

$$I_1(a,b) = \frac{ab}{2(a-b)} + \frac{a^2b^2}{2(a-b)^2}\left[f(a)-f(b)\right] + \frac{a^2 b}{(a-b)^2}\left[g(a)-g(b)\right],$$

$$I_2(a,b) = -\frac{ab}{2(a-b)}\left[f(a)-f(b)\right].$$

The expression of $g(\tau/\lambda)$ is given by

$$g(\tau) = \begin{cases} \sqrt{\tau-1}\arcsin\sqrt{\frac{1}{\tau}} & \text{for } \tau \geq 1, \\ \frac{\sqrt{1-\tau}}{2}\left(\log\frac{1+\sqrt{1-\tau}}{1-\sqrt{1-\tau}} - i\pi\right) & \text{for } \tau < 1. \end{cases}$$

References

1. G. Aad et al. (ATLAS Collaboration), Phys. Lett. B **716**, 1 (2012)
2. S. Chatrchyan et al. (CMS Collaboration), Phys. Lett. B **716**, 30 (2012)
3. (ATLAS Collaboration), ATLAS-CONF-2014-009
4. (CMS Collaboration), CMS-HIG-13-001
5. P. Ade et al. (PLANCK Collaboration), arXiv:1303.5076 [astro-ph.CO]
6. N. Jarosik, C.L. Bennett, J. Dunkley, B. Gold, M.R. Greason, M. Halpern, R.S. Hill, G. Hinshaw et al., Astrophys. J. Suppl. **192**, 14 (2011). arXiv:1001.4744 [astro-ph.CO]
7. K. Griest, M. Kamionkowski, Phys. Rep. **333**, 167 (2000)
8. G. Bertone, D. Hooper, J. Silk, Phys. Rep. **405**, 279 (2005)
9. G. Jungman, M. Kamionkowski, K. Griest, Phys. Rep. **267**, 195 (1996)
10. H.-C. Cheng, J.L. Feng, K.T. Matchev, Phys. Rev. Lett. **89**, 211301 (2002)
11. V. Silveira, A. Zee, Phys. Lett. B **161**, 136 (1985)
12. A. Hill, J.J. van der Bij, Phys. Rev. D **36**, 3463 (1987)
13. J. McDonald, Phys. Rev. D **50**, 3637 (1994). arXiv:hep-ph/0702143
14. C.P. Burgess, M. Pospelov, T. ter Veldhuis, M.C. Bento, O. Bertolami, R. Rosenfeld, L. Teodoro, Phys. Rev. D **62**, 041302 (2000). arXiv:astro-ph/0003350
15. V. Barger, P. Langacker, M. McCaskey, M.J. Ramsey-Musolf, G. Shaughnessy, Phys. Rev. D **77**, 035005 (2008). arXiv:0706.4311 [hep-ph]
16. S. Andreas, T. Hambye, M.H.G. Tytgat, JCAP **0810**, 034 (2008). arXiv:0808.0255 [hep-ph]
17. C.E. Yaguna, JCAP **0903**, 003 (2009). arXiv:0810.4267 [hep-ph]
18. X.-G. He, T. Li, X.-Q. Li, J. Tandean, H.-C. Tsai, Phys. Rev. D **79**, 023521 (2009). arXiv:0811.0658 [hep-ph]
19. X.-G. He, T. Li, X.-Q. Li, J. Tandean, H.-C. Tsai, Phys. Lett. B **688**, 332 (2010). arXiv:0912.4722 [hep-ph]
20. A. Bandyopadhyay, S. Chakraborty, A. Ghosal, D. Majumdar, JHEP **1011**, 065 (2010). arXiv:1003.0809 [hep-ph]
21. S. Andreas, C. Arina, T. Hambye, F.-S. Ling, M.H.G. Tytgat, Phys. Rev. D **82**, 043522 (2010). arXiv:1003.2595 [hep-ph]
22. Y. Mambrini, Phys. Rev. D **84**, 115017 (2011). arXiv:1108.0671 [hep-ph]
23. A. Biswas, D. Majumdar, Pramana **80**, 539 (2013). arXiv:1102.3024 [hep-ph]
24. Y.G. Kim, K.Y. Lee, S. Shin, JHEP **0805**, 100 (2008). arXiv:0803.2932 [hep-ph]
25. M.M. Ettefaghi, R. Moazzemi, JCAP **1302**, 048 (2013). arXiv:1301.4892 [hep-ph]
26. M. Fairbairn, R. Hogan, JHEP **1309**, 022 (2013). arXiv:1305.3452 [hep-ph]
27. M. Aoki, S. Kanemura, O. Seto, Phys. Lett. B **685**, 313 (2010)
28. Y. Cai, X.G. He, B. Ren, Phys. Rev. D **83**, 083524 (2011). arXiv:1102.1522 [hep-ph]
29. O. Fischer, J.J. van der Bij, JCAP **1401**, 032 (2014)
30. E. Ma, Phys. Rev. D **73**, 077301 (2006). arXiv:hep-ph/0601225
31. L. Lopez Honorez, E. Nezri, J.F. Oliver, M.H.G. Tytgat, JCAP **0702**, 028 (2007). arXiv:hep-ph/0612275
32. D. Majumdar, A. Ghosal, Mod. Phys. Lett. A **23**, 2011 (2008). arXiv:hep-ph/0607067
33. M. Gustafsson, E. Lundstrom, L. Bergstrom, J. Edsjo, Phys. Rev. Lett. **99**, 041301 (2007). arXiv:astro-ph/0703512
34. Q.-H. Cao, E. Ma, G. Rajasekaran, Phys. Rev. D **76**, 095011 (2007). arXiv:0708.2939 [hep-ph]
35. E. Lundstrom, M. Gustafsson, J. Edsjo, Phys. Rev. D **79**, 035013 (2009). arXiv:0810.3924 [hep-ph]
36. S. Andreas, M.H.G. Tytgat, Q. Swillens, JCAP **0904**, 004 (2009). arXiv:0901.1750 [hep-ph]
37. L. Lopez Honorez, C.E. Yaguna, JHEP **1009**, 046 (2010). arXiv:1003.3125 [hep-ph]
38. L. Lopez Honorez, C.E. Yaguna, JCAP **1101**, 002 (2011). arXiv:1011.1411 [hep-ph]
39. T.A. Chowdhury, M. Nemevsek, G. Senjanovic, Y. Zhang, JCAP **1202**, 029 (2012). arXiv:1110.5334 [hep-ph]
40. D. Borah, J.M. Cline, Phys. Rev. D **86**, 055001 (2012). arXiv:1204.4722 [hep-ph]
41. E. Aprile et al. (XENON100 Collaboration), Phys. Rev. Lett. **109**, 181301 (2012). arXiv:1207.5988 [astro-ph.CO]
42. D. S. Akerib et al. (LUX Collaboration), Phys. Rev. Lett. **112**, 091303 (2014). arXiv:1310.8214 [astro-ph.CO]
43. R. Agnese et al. (CDMS Collaboration), Phys. Rev. D **88**, 031104 (2013). arXiv:1304.3706 [astro-ph.CO]
44. R. Agnese et al. (CDMS Collaboration), Phys. Rev. Lett. **111**, 251301 (2013). arXiv:1304.4279 [hep-ex]
45. R. Bernabei et al. (DAMA Collaboration), Eur. Phys. J. C **56**, 333 (2008). arXiv:0804.2741 [astro-ph]
46. R. Bernabei et al. (DAMA and LIBRA Collaborations), Eur. Phys. J. C **67**, 39 (2010). arXiv:1002.1028 [astro-ph.GA]
47. C.E. Aalseth et al, (CoGeNT Collaboration), Phys. Rev. Lett. **106**, 131301 (2011)
48. G. Angloher, M. Bauer, I. Bavykina, A. Bento, C. Bucci, C. Ciemniak, G. Deuter, F. von Feilitzsch et al., Eur. Phys. J. C **72**, 1971 (2012). arXiv:1109.0702 [astro-ph.CO]
49. J.F. Gunion, H.E. Haber, Phys. Rev. D **67**, 075019 (2003). arxiv:hep-ph/0207010
50. K. Kannike, Eur. Phys. J. C **72**, 2093 (2012). arXiv:1205.3781 [hep-ph]
51. J. Beringer et al. (Particle Data Group), Phys. Rev. D **86**, 010001 (2012)
52. E.W. Kolb, M. Turner, *The Early Universe* (Westview Press, Boulder, 1990)
53. A. Biswas, D. Majumdar, A. Sil, P. Bhattacharjee, JCAP **1312**, 049 (2013). arXiv:1301.3668 [hep-ph]

54. A. Arhrib, R. Benbrik, N. Gaur, Phys. Rev. D **85**, 095021 (2012). arXiv:1201.2644 [hep-ph]
55. B. Swiezewska, M. Krawczyk, Phys. Rev. D **88**, 035019 (2013). arXiv:1212.4100 [hep-ph]
56. A. Goudelis, B. Herrmann, O. Stal, JHEP **1309**, 106 (2013). arXiv:1303.3010 [hep-ph]
57. P. Posch, Phys. Lett. B **696**, 447 (2011). arXiv:1001.1759 [hep-ph]
58. G. Bhattacharyya, D. Das, P.B. Pal, M.N. Rebelo, JHEP **1310**, 081 (2013). arXiv:1308.4297 [hep-ph]
59. A. Denner et al., Eur. Phys. J. C **71**, 1753 (2011). arXiv:1107.5909 [hep-ph]
60. Y. Kajiyama, H. Okada, T. Toma, Eur. Phys. J. C **73**, 2381 (2013). arXiv:1210.2305 [hep-ph]
61. R. Barbieri, L.J. Hall, V.S. Rychkov, Phys. Rev. D **74**, 015007 (2006). arxiv:hep-ph/0603188
62. E. Aprile (XENON1T Collaboration), in *Proceedings of DM2012*. arXiv:1206.6288 [astro-ph.IM]
63. R. Agnese et al. (SuperCDMS Collaboration), Phys. Rev. Lett. **112**, 241302 (2014). arXiv:1402.7137 [hep-ex]
64. (ATLAS Collaboration), ATLAS-CONF-2012-162
65. J.F. Gunion, H.E. Haber, G.L. Kane, S. Dawson, Front. Phys. **80**, 1 (2000)
66. A. Djouadi, Phys. Rep. **459**, 1 (2008). arXiv:hep-ph/0503173
67. A. Djouadi, Phys. Rep. **457**, 1 (2008). arXiv:hep-ph/0503172